INVESTIGATIONS OF QCD HADRONIZATION USING JETS MEASURED AT $\sqrt{s} = 8$ TeV WITH THE ALICE DETECTOR.

A Dissertation Presented for the

Doctor of Philosophy

Degree

The University of Tennessee, Knoxville

Andrew John Castro

March 2019

Chapter 1

Quantum Chromodynamics

In 1968 deep inelastic scatterings performed at the Stanford Linear Accelerator Center showed that the proton had internal structure[1] called partons at the time. Within a decade of this discovery the partons were broken into two categories: the mass carrying fermions were known as the quarks and the gauge boson force carriers were called gluons. The interactions of these two types of particles were described by the quantum field theory known as quantum chromodynamics (QCD) and by the SU(3) symmetry group. SU(3) guarantees that color charge is conserved and this results in quarks grouping together into 'colorless' hadrons.

1.1   The QCD Lagrangian

QCD is the strongest of the known fundamental forces. It is a gauge field theory described by the Lagrangian density

$$\mathcal{L} = -\frac{1}{4}F_{\mu\nu}^{\alpha}F_{\alpha}^{\mu\nu} - \alpha_s(\bar{q}_j\gamma^{\mu}T_{\alpha}q_j)G_{\alpha}^{\mu} + \bar{q}_j(i\gamma^{\mu}\partial_{\mu} - m)q_j \qquad (1.1)$$

where q and $\bar{q}$ represent the color anti-color fields summed over color j, α_s is the strong coupling strength, γ^{μ} is the Dirac gamma matrix, G_{α}^{μ} is the gauge field for color α, is similar in analogy to the $\mathbf{W}$ matrix from the electroweak theory. $F_{\mu\nu}^{\alpha}$ is the field strength tensor and it describes the gluon interactions. The first term of the Lagrangian is the gluon contribution

and carries no mass term. The second term of the Lagrangian describes how quarks and gluons interact with each other. The final term describes quark interactions and the coupling between them and will be explored further in this thesis.

At short distances, less than 0.2 *fm*, the strong coupling constant becomes exceedingly small and second term of the Lagrangian displays an important property known as asymptotic freedom[2].

$$\alpha_s = \frac{1}{\beta_0 \ \ln(Q^2/\Lambda^2)} \tag{1.2}$$

where α_s is the strong coupling constant, Q^2 is the momentum transfer between two interacting partons, and Λ^2 is a cutoff below which QCD phenomena are strongly suppressed and β_0 is a correction factor.
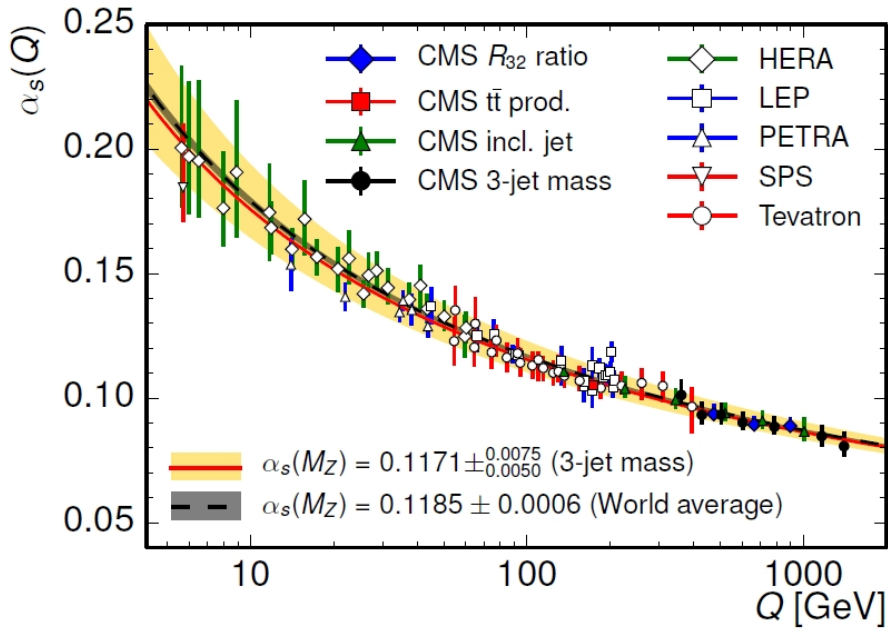

Figure 1.1: Strong coupling constant (α_s) as a function of the momentum transfer (Q)[3].

1.2 Jets

Hard probes (large Q^2 interactions), are produced in the earliest stages of a high energy collision when the largest momentum transfer processes occur. As two highly energetic

partons propagate away from one another, in a back-to-back fashion, they will instigate a shower of daughter partons via gluon radiation and the generation of low-mass $q\bar{q}$ pairs. These daughter partons will go on to form hadrons and the clustering of theses hadrons is colloquially known as a 'jet'. If the jet was created in a high energy experiment the final state hadrons will be recoreded as tracks in a tracking detector or energy deposets in a calorimeter. This process is shown in Figure 1.2.
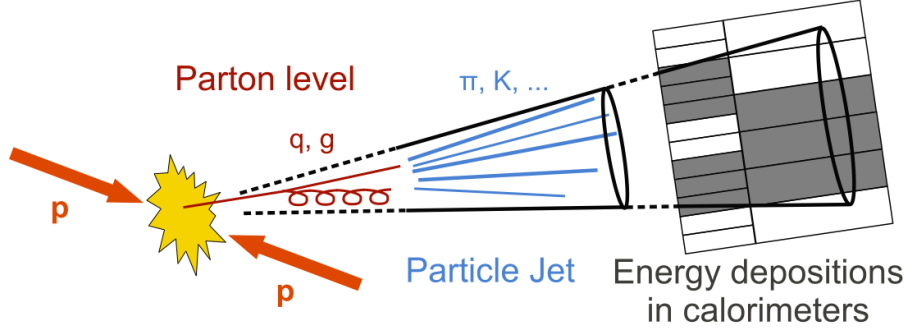
Figure 1.2: Diagram showing a jet created by two partons under going a hard scattering, forming into hadrons, and detected in a calorimeter[4].

The physicist James Daniel Bjorken postulated that a correlation could be surmised by summing over the final state transverse momentum of the hadrons that form a jet to the parton that initiated the hard scattering[5][6]. This has lead to jets becoming the work-horse for both experimentalists and theoreticians over the past 30 years in probing QCD phenomena. This thesis makes use of jets as an important probe of QCD and the following sections are devoted to developing a background for both the theoretical and experimental treatment of jet physics. The following sections will be devoted to how jets are produced from a physics point-of-view and the latest results which this thesis compares to.

1.2.1   Jet Production and the Factorization Theorem

Due to confinement bare quarks are unobserved, therefore experimentalists must probe QCD interactions by detecting the color neutral final state hadrons measured in collider experiments. Fortunately, the factorization theorem (Equation 1.3) allows for the final state jet cross section to be broken into a number of steps that can either be calculated

pertubativlely using pQCD or modeled phenomenologically. Using the factorization theorem the jet cross section in a pp collision is,

$$d\sigma^{pp \to jet} \sim f_{a/A}(x_1, Q^2) \otimes f_{b/B}(x_2, Q^2) \otimes d\sigma_{ab \to c+X}(x_1, x_2) \otimes D_{c \to h/jet}(z, Q^2) \qquad (1.3)$$

- $f_{a/A}(x_1, Q^2)$ and $f_{b/B}(x_2, Q^2)$ are the parton distribution functions (PDF) that describe the probability of finding parton, a or b, within nuclei, A and B, with a given momentum fraction, $x = p_{parton}/p_{hadron}$ as a function of Q^2.

- $d\sigma_{ab \to c+X}(x_1, x_2)$ is the pQCD parton-parton cross section due to the hard scattering of the two partons, a and b, to and intermediate parton (c).

- $D_{c \to h/jet}(z, Q^2)$ is the fragmentation function (FF) that describes the probability the an outgoing parton, c, fragments and hardonizes into a final state hadron, h, within a jet with momentum fraction, $z \equiv p_{hadron}/p_{parton}$.

Figure 1.3 shows a timeline of a pp collision broken into the relevant steps in accordance to the factorization theorem. One of the best places to fundamentally test QCD phenomena using hard probes, i.e. jets, are with high energy hadron colliders such as those found at CERN[1], Fermilab, and BNL. The time scale that a hard probe is created in a high energy collision is on the order of $\tau \approx 1/p_T \approx 0.1$ fm/c which probes the initial state these interactions. The factorization theorem allows for a high level of agreement between the QCD theory of nature and experimental observables but to ascertain this connection we should discuss each term of the factorization theorem in more depth.

Parton Distribution Functions

The PDF occurs twice in Equation 1.3 due to the two partons that will undergo the hard scattering being confined in two different protons. PDFs may be thought of as conveying the structure of a nucleon in terms of the number of flavored quarks or gluons ($u(x)$, $d(x)$,

---

[1]Discussed in detail in Chapter 3
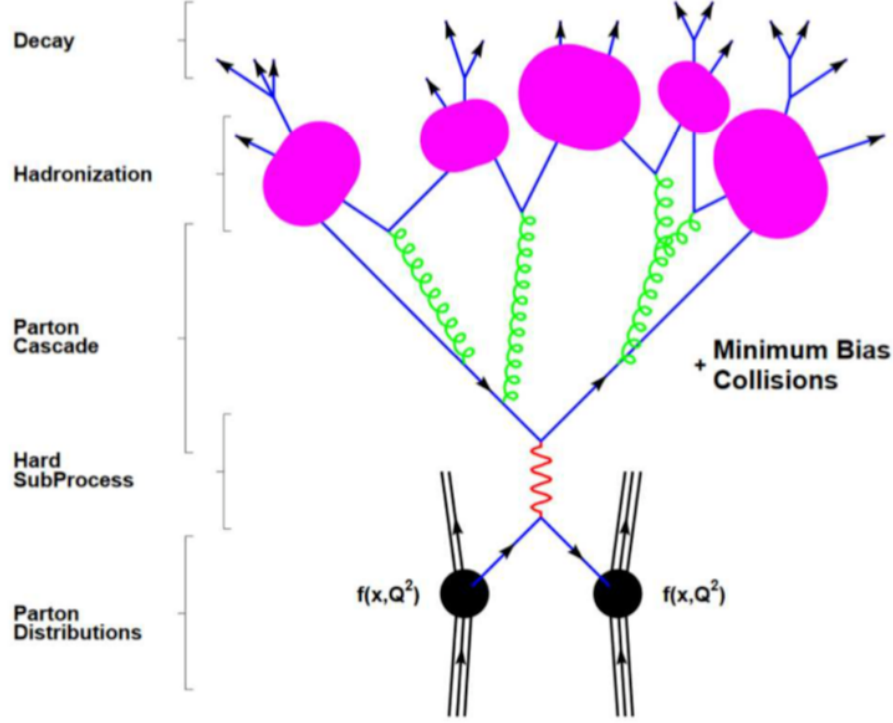
Figure 1.3: Timeline of a proton-proton collision. Starting from the bottom, two partons confined within the colliding protons have a hard interaction. The outgoing partons will induce partonic showers by radiating quarks and gluons. The partonic showers will eventually form into final state hadrons due to confinement which are measured in high energy experiments[7].

$s(x)$, $\overline{u}(x)$, $\overline{d}(x)$, $\overline{s}(x)$, $g(x)$) and must obey certain constraints and summation rules. In the case of a proton, with electric charge ($e = +1$),

$$+1 = \frac{2}{3}\int_0^1 [u(x) - \overline{u}(x)]dx - \frac{1}{3}\int_0^1 [d(x) - \overline{d}(x)]dx \tag{1.4}$$

and isospin ($I = 1/2$),

$$\frac{1}{2} = \frac{1}{2}\int_0^1 [u(x) - \overline{u}(x)]dx - \frac{1}{2}\int_0^1 [d(x) - \overline{d}(x)]dx \tag{1.5}$$

have a solution,

$$\int_0^1 [u(x) - \overline{u}(x)] = 2 \tag{1.6}$$

$$\int_0^1 [d(x) - \overline{d}(x)]dx = 1 \tag{1.7}$$

5

This corresponds to the classical partonic view that protons contained two up quarks and a down quark, similarly the neutron, with charge $e = 0$ and isospin $I = -1/2$, can be shown that it compromises two down quarks and a up quark. Naively, we could assume that the three quarks composing a proton would each carry a momentum fraction of approximately 1/3 the total momentum of a proton. However, high energy deep inelastic scattering experiments conducted at the Stanford Linear Collider in the 1960's[8] measured the momentum carried by the three quarks only accounting for about 1/2 the total proton momentum. This lead to a more complex and dynamic model of the proton structure with the other half of the proton momentum being occupied by neutral partons which would eventually become known as gluons.
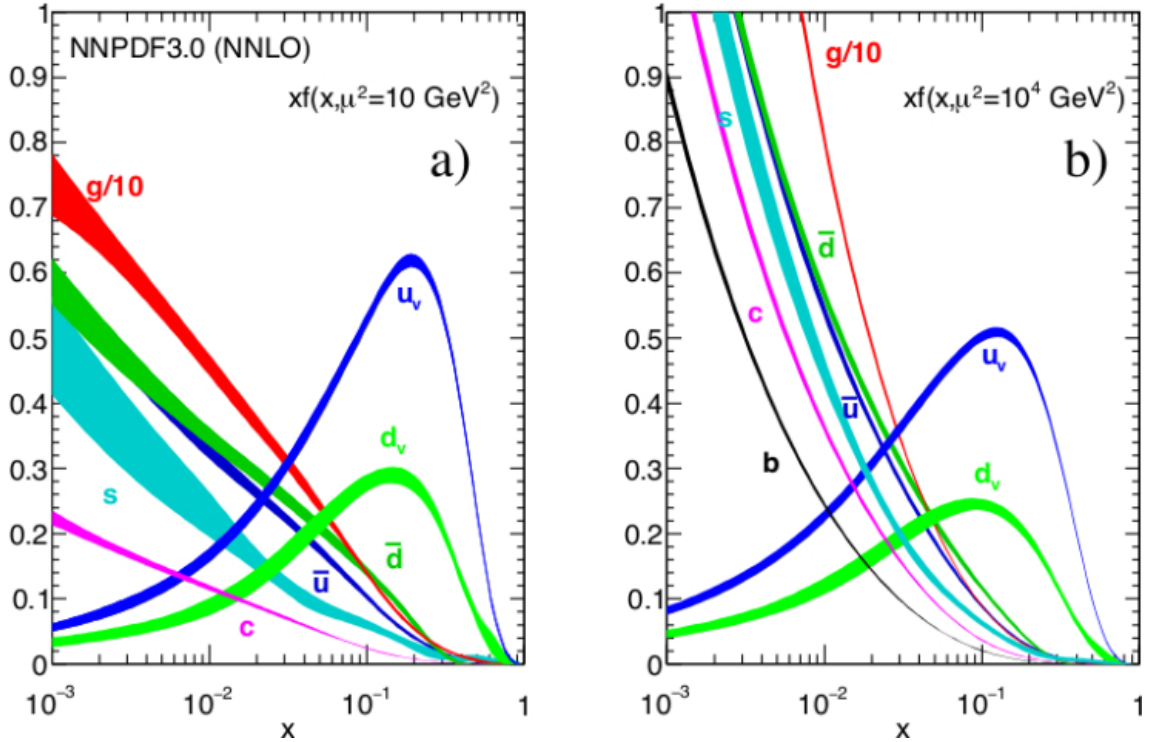

Figure 1.4: Proton PDF at $Q^2 = 10$ GeV (left) and $Q^2 = 10$ TeV (right) from the NNPDF Collaboration[9].

Measuring the structure of the partons making up a nucleon is a major endeavor by both theoreticians and experimentalists. Two of the most popular PDFs available to physicists are the CTEQ[10] (Coordinated Theoretical-Experimental Project on QCD) and the NNPDF[11] (Neural Network Parton Distribtuion Function) sets. Figure 1.4 shows the proton PDF as

a function of the momentum fraction for two energy ranges, at high values of x the the two up quarks account for about 2/3 of the momentum fraction while down quark accounts for about 1/3 the total momentum, these quarks are collectively called the valence quarks. At high energies, low values of x, we see that the proton has non negligible contributions from gluons, anti-quarks, strange, and even charm quarks, these are collectively known as the sea partons. Today, the modern picture of a protons structure is that it is mostly composed of gluons and sea quarks at low values of x and this domination only increases as a function of Q^2[12].

Parton-Parton Cross-Section

The parton-parton cross section can be calculated using perturbation theory. To the zeroth order in α_s this cross-section would be a simple quark-antiquark annihilation and would be calculable using Feynman diagrams as seen in Figure 1.5[13]. Higher ordered contributions, such as the creation of virtual gluons, require the hard cross-section to be expanded as a series in terms of α_s. Calculations of the hard cross section that incorporate these higher order terms are known as *next-to-leading order* (NLO) with N denoting the number of terms after the leading order that have been included in the cross-section calculation. Various calculations of the hard cross-section of different QCD processes have been performed over the years typically using either power series or logarithmic expansions of α_s[14] and corrections for LO, NLO, and even NNLO constitutes a very active field in high energy physics.
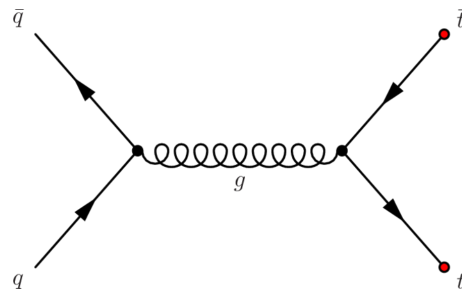

Figure 1.5: Lowest order quark-antiquark annihilation to top-antitop pair[15].

Perturbative techniques of the hard cross-section have been extremely successfully in describing jet features in hadronic collisions[12].

Hadronization

Hadronization is the process by which the colored pQCD partons of form into colorless non-pQCD hadrons and represents a significant barrier in progressing jet physics. This is due to the fact that hadronization encompass several smaller processes which in themselves are hard to characterize. Thus, like PDFs, an accurate description of hadronization requires a phenomenological approach by which experimental results help complement theoretical calculations. Jet production via hadronization[16] follows two distinct stages. First, the partons that underwent a hard scattering start to emit radiation via gluon bremsstrahlung up until time, $t < Q^2$, this is known as the parton cascade. The parton cascade is the precursor of what will become a jet as most of the radiation generated will travel in the same direction as the initial hard scattered parton. However, this immediately poses an issue in jet physics as radiation generated at a wide angle away from the momentum axis of the inital hard scattered parton will not be associated with the jet.
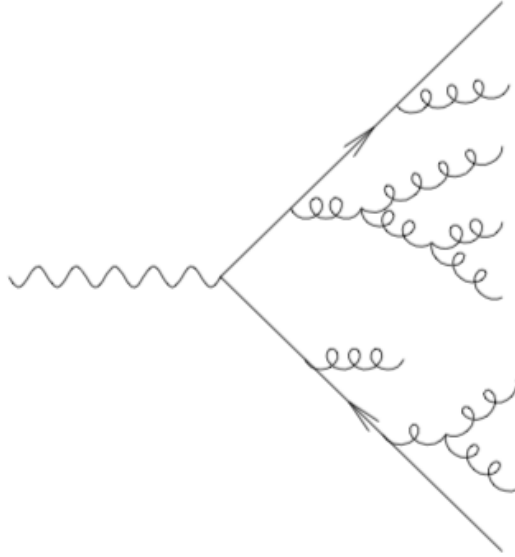

Figure 1.6: Parton cascade in a hadronic collision[16].

After the cascade has ended the partons must fragment into color neutral hadrons. Their are two main phenomenological models used to describe the hadron forming process, the Lund String Model and the Cluster Hadronization Model. The QCD potential is,

$$V(r) = -\frac{\alpha_s}{r} + \sigma\,r \tag{1.8}$$

where the first term of Equation 1.8 goes as the Coulomb potential with a 1/r dependence and is the dominate term at short distance and the second term has a string-like potential with σ referring to a string-like tension. The Lund String Model ignores gluon radiation and has fragmentation occur via breaking the string tension with the production of $q\bar{q}$ sea quarks. The created sea quarks will carry some momentum fraction, z, of the initial parton until z falls below some cutoff. Figure 1.7 shows a two quarks undergoing a string breaking, each of the quarks initiating the string breaking will combine with a sea quark in an iterative manner to form hadrons.
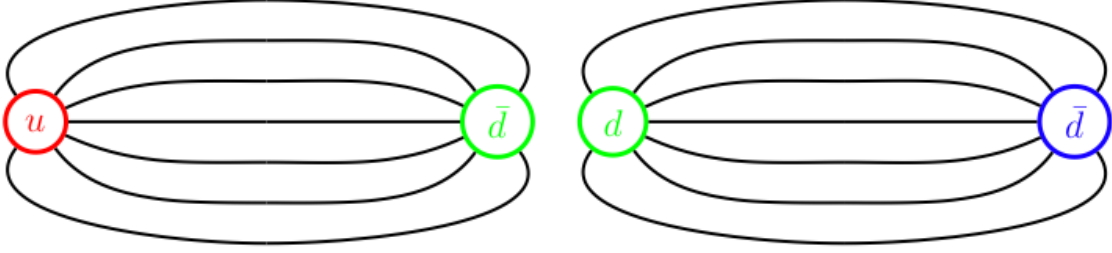
Figure 1.7: $u\bar{d}$ generating a $d\bar{d}$ pair via string breaking which will form color neutral hadrons, black lines show the string like equipotentials.[17].

The Cluster Hadronization Model has gluons splitting after the parton cascade phase into $q\bar{q}$ pairs. These pairs will form color-singlet clusters with other neighboring quarks in phase-space. These color-singlets will typically be a few GeV/c^2 in mass and are treated as excited meson resonances. These psuedo-resonances will decay via their normal branching ratios into the stable hadrons[18].

Fragmentation

Similar to how a PDF quantitatively describes the structure of a nucleon the FF quantitatively describes the hadronization process. The FF is also similar to the PDF in that it is also a probability distribution, thus it follows the probabilistic rule that,

$$\sum \int z D_{c \to h/jet}(z, Q^2)dz = 1 \tag{1.9}$$

Ideally, the fractional momentum of the hadrons created from the fragmenting parton, $z \equiv p_{hadron}/p_{parton}$. Due to the confinement of partons we must use a a suitable substitution for measuring the FF. The Parton-Hadron Duality[19] states that a hadron found near the center of a jet should encompass the quantum numbers and kinematic properties associated with the hard scattered quark that initiated the jet. Thus we can measure the fragmentation function as $z = p_{hadron}/p_{jet}$. The formulation of the FF as a fractional energy carried by the hadrons in a jet was a breakthrough in pQCD techniques and is analogous to how an electron passing through an absorber creates photon showers with these photons generating conversion electrons until the total energy has been dissipated into the material.
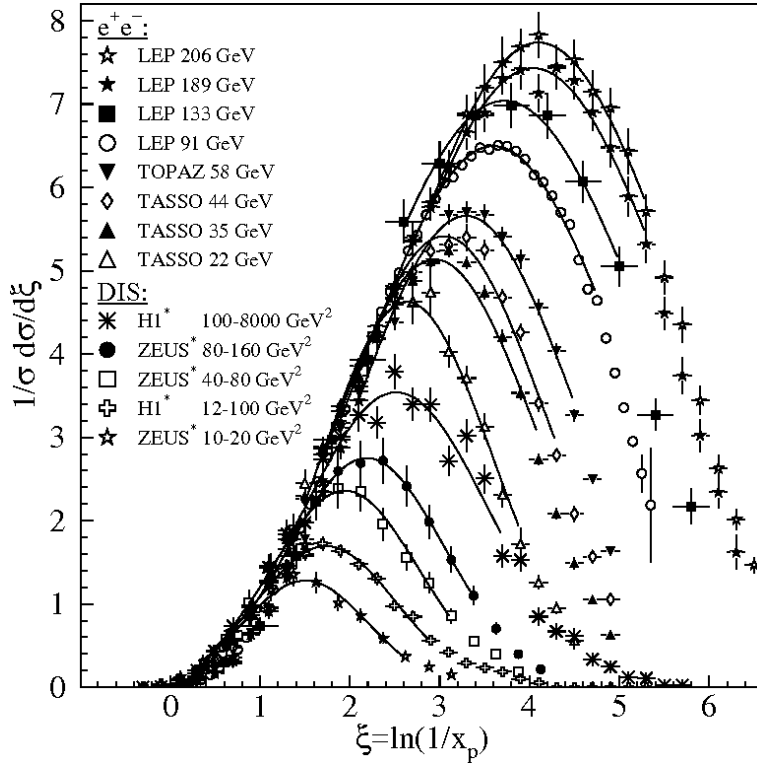

Figure 1.8: Fragmentaion Functions from e^+e^- and DIS experiments with fits[20].

Figure 1.8 is the FF in terms of the Gaussian equation, $z \, dN/dz = -dN/d\xi$ with $\xi = -ln \, 1/z$. The observation that the Gaussian peaks of Figure 1.8 along with the suppression of the FF at low z values due to gluon coherence were predicted by pQCD.

1.3 Jet Finding Algorithams

A jet arises from the fragmentation of a hard parton to final state hadrons. However, grouping the hadrons together into a jet is a non-trivial task and jet finding algorithms are deployed in order to achieve this objective. Early on in jet physics, both theoreticians and experimentalists used a wide variety of jet finders that made comparisons between experiments or to theoretical calculations nearly impossible[21]. For example, a radiated gluon that splits into a quark anti-quark pair may become one or two jets depending on the angular separation and the algorithm used. Early jet finders tended to be sensitive to soft particles or could give widely varying yields to the number of jets in an event. In 1990, the Snowmass Accord[22] was held in order to standardize the definition of a jet between experimentalists and theoreticians. The agreement maintained that any algorithm that clusters particles into a jet must be both infrared and collinear safe (IRC).
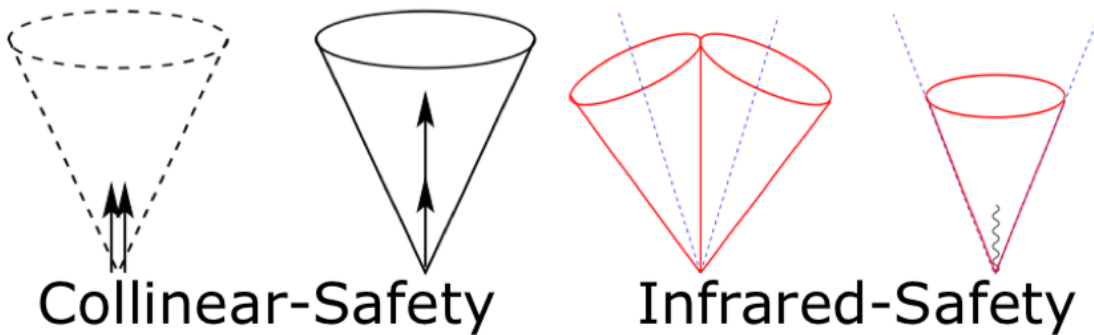
Figure 1.9: Cartoon showing Collinear and Infrared safe jet candidates[23].

Collinear safety ensures that a high-p_T particle split into two or more particles should not influence the kinematics of a hard jet, this makes the jet finders insensitive to how hadrons are grouped together. Infrared safety in turn requires that the emission of soft radiation should not affect the properties of a jet, this makes jets returned by the algorithm independent of soft physics and a true signature of a hard process. Both of these processes are shown in Figure 1.9. After the adoption of these standards from the Snowmass Accord, old algorithms that violated these rules were patched and new jet finders were developed to comply with IRC safety. The most prevalent jet finding algorithms today fall into two categories: cone algorithms and sequential recombination/clustering algorithms.

1.3.1 Cone Algorithms

Cone algorithms made up the bulk of early jet finders. The only IRC safe cone algorithm still in use today is the seedless infra-red safe cone algorithm (SIScone). SIScone defines a cone of radius, R, around the highest momentum particle in the coordinates of (η, ϕ)[2], this is the proto-jet. SIScone then proceeds through an iterative process of finding all the particles withing the jet radius such that $R \leq \sqrt{\phi^2 + \eta^2}$ and calculates a new jet center based on these particles momenta and a new weighted jet axis(η, ϕ). If the new center matches the proto-jet center, the proto-jet is tagged as a stable jet, all the particles in that jet are removed, and SIScone moves onto the next highest p_T particle. Cone algorithms tend to be unpopular due to being computationally expensive, they are hard to implement theoretically, and can give results not calculable in pertubation theory.

1.3.2 Sequential/Recombination Algorithms

The other class of jet finders are the sequential/recombination algorithms, which are favored by experimentalists, theoreticians and are IRC safe. There are three types of sequential/recombination algorithms: k_T, Anti-k_T, and the Cambridge/Aachen jet finders, with k_T referring to the transverse momentum of particle. All of the algorithms use a similar method, first they find the distance between every pair of particles, $d_{i,j}$, such that

$$d_{i,j} = min[p_{T,i}^a, p_{T,j}^a] \, \frac{\Delta_{ij}^2}{R^2} \tag{1.10}$$

where $p_{T,i}^a$ is the transverse momentum of particle i, a is free parameter that is set based on which algorithm is used, $\Delta_{ij}^2 = (\eta_i - \eta_j)^2 + (\phi_i + \phi_j)^2$ is the distance between the particles, and R is the radius of the jet. A second distance is defined in the sequential/recombination algorithm scheme,

---

[2]It is possible to use a Cartesian coordinate system in particle colliders, with the z-component referring to points along the beam axis while the xy-plane is perpendicular to the beam axis. However, this system is not invariant under a Lorentz boost. Therefore it is more useful to use the cylinrical-like coordinates of psuedorapidity (η) and the azimuth angle (ϕ). Psuedorapidity may be thought of as the polar angle in a cylindrical coordinate system with $\eta = 0$ when the polar angle is perpendicular to the beam axis and $\eta = $ inf along the beam axis. ϕ is the azimuth angle that rotates around the beam axis. Both, η and ϕ are invariant for Lorentz boosts along the beamline and allow for easy comparisons between the center-of-mass frame and the laboratory frame of a high energy collision.

$$d_{i,B} = p_{T,i}^a \tag{1.11}$$

this is the distance between a given particle i and the beam axis. Sequential/Recombination algorithms find the set of all particles, $d_{i,j}, d_{i,B}$, such that if $d_{i,B}$ is the minimum for particle i it is tagged as a jet and removed from the list. If $d_{i,j}$ are a minimum for particles i and j these two particles are merged together into a new particle (ij) and a new minimum is found between (ij) and particle k until all the particles are either merged into jets or the minimization function is no longer satisfied.

k_T Algorithm

The k_T algorithm sets the value a to 2, this results in a minimization function,

$$d_{i,j} = min[p_{T,i}^2, p_{T,j}^2] \frac{\Delta_{ij}^2}{R^2} \tag{1.12}$$

which clusters low momentum particles first, making this algorithm susceptible to the underlying event (UE) or pile-up (PU). Thus the k_T algorithm is good at estimating any background present in a high energy collision.

Anti-k_T Algorithm

The Anti-k_T algorithm sets the value a to -2, resulting in a minimization function,

$$d_{i,j} = min\left[\frac{1}{p_{T,i}^2}, \frac{1}{p_{T,j}^2}\right] \frac{\Delta_{ij}^2}{R^2}. \tag{1.13}$$

The minimization function is dominated by high-p_T particles, thus the area and axis of a jet is only slightly perturbed by soft particles. This makes the Anti-k_T algorithm robust in jet finding with events having a UE and PU. The Anti-k_T algorithm is the default jet finding algorithm used at the Large Hadron Collider and is the one used in this thesis.

Cambridge/Aachen Algorithm

The Cambridge/Aachen algorithm sets a to 0 and this results in a minimization function of,

$$d_{i,j} = \frac{\Delta_{ij}^2}{R^2} \tag{1.14}$$

which makes it independent of particle momentum and sensitive to PU and UE. Due to the fact that the Cambridge/Aachen algorithm is only dependent on the particle coordinate it is most useful in studying jet structure.
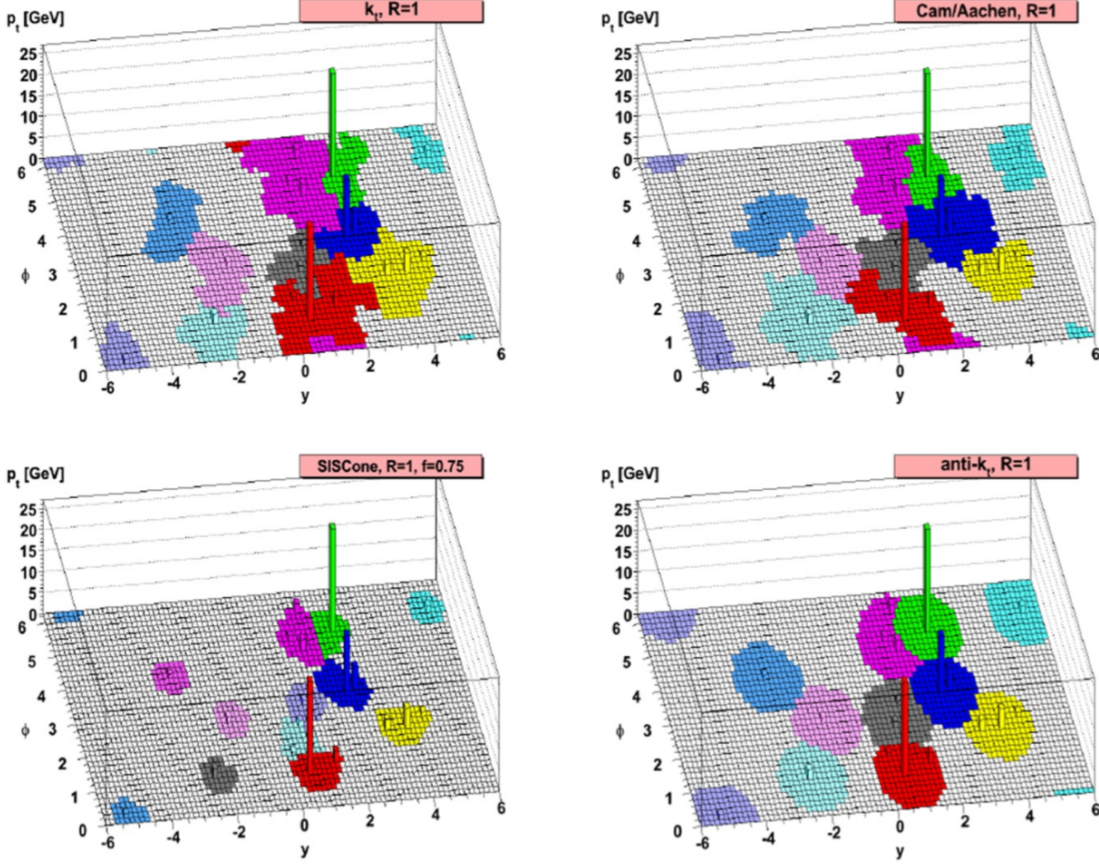
Figure 1.10: Lego plot of all four jet finders used on a single event with R = 1 jet radius[21].

Figure 1.10 shows the jets found in a single event using all four jet finding algorithms. It should be noted that the Cambridge/Aachen and k_T algorithms have highly irregular and large shapes, making them both susceptible to the presence of a UE, while SIScone finds an additional jet due to splitting. The Anti-k_T algorithm finds circular jets which demonstrates its robustness to hard radiation.

Once a stable jet is found, a recombination scheme is deployed in order to garner the jet kinematics. By adding the 4-vector, $\boldsymbol{p}^\mu = (\boldsymbol{E}, \boldsymbol{p}_x, \boldsymbol{p}_y, \boldsymbol{p}_Z)$, for all of the associated particles

composing a jet, we may obtain the jet momentum, energy, coordinates, etc[3]. In a particle collider with the tracks from a tracking detector measuring particle momentum and the towers of a calorimeter measuring particle energy we obtain the following relationships

$$p_T^{jet} = \sum_{particles} p_T = \sum_{tracks} p_T \tag{1.15}$$

$$E^{jet} = \sum_{particles} E = \sum_{towers} E \tag{1.16}$$

$$\eta^{jet} = \frac{1}{2} \ln \left(\frac{|\boldsymbol{p}^{jet}| + p_L^{jet}}{|\boldsymbol{p}^{jet}| - p_L^{jet}} \right) \tag{1.17}$$

$$\tan \phi^{jet} = \frac{p_y^{jet}}{p_x^{jet}} \tag{1.18}$$

where p_L refers to the longitudinal momentum which is the momentum component parallel to the beam axis. This method of adding the 4-vector of the particles composing the jet together in order to gain the jet kinematics is known as the E-scheme[24].

1.3.3 FastJet

FastJet[24] is a `C++` software package that performs jet finding. Due to the computational efficiency, ease of use, and straight forward implementation, FastJet is the de-facto preferred jet finder used by theoreticians and all current high energy experiments. It implements the four previously discussed jet finders along with both the E-scheme and a boost invariant p_T scheme (BIpt-scheme) for recombination. The BIpt-scheme obtains the jet momentum and energy in the same manner as the E-scheme but uses a weighted average to find the jet coordinates,

$$\eta^{Jet} = \sum_{particle} \frac{p_T^{particle}}{P_T^{jet}} \eta^{particle} \tag{1.19}$$

---

[3]For a review of relativistic kinematic see Appendix ...

$$\phi^{jet} = \sum_{particle} \frac{p_T^{particle}}{P_T^{jet}} \phi^{particle} \tag{1.20}$$

In addition to basic jet measurements, FastJet contains a number of advance features, which allows it to be used to study jet area, jet substructure, and jet background subtraction[25].

1.4 Monte-Carlo Generators

Monte-Carlos (MC) allow for the simulation of high energy events on a statistical basis. Particle level generators use different phenomenological models of the factorization theorem in order to simulate the energy, momentum, particle species, multiplicity, and direction of travel expected in a high energy collision. In order to validate an analysis the particle level simulations are further propagated through a detector level simulation of an experiment, such as Geant3[26], in order to negate detector effects on the output observables from the MC simulation. In this section only the particle level simulations used in the thesis are discussed.

1.4.1 PYTHIA

PYTHIA[27], is a `C++` Monte Carlo software tool-kit used to model proton-proton collisions. The package uses pre-defined parton distribution functions as input afterwards it simulates the partonic showers and radiation due to a hard scattering by generating the LO scattering matrix elements. Hadronization is performed in PYTHIA using the Lund String Model. After which relative branching ratios are used to statistically throw the decay modes of the hadrons until they are stabilized.

PYTHIA underestimates jet production due to the limitations of using LO calculations. Therefore, it uses an arbitrary value (K-factor) to make NLO corrections to the LO cross section. The K-factor is defined as,

$$K = \frac{\sigma_{NLO}}{\sigma_{LO}}. \tag{1.21}$$

NLO corrections to the cross-section will not match experimental results, PYTHIA implements additional phenomenological adjustments used to better match data. PYTHIA encompass these corrections into sets known as 'tunes', with PYTHIA 6.4 Perugia-2010 tune being used for this analysis[28].

1.4.2 PHOJET

PHOJET is a `FORTRAN 77` Monte Carlo simulator used to model proton-proton collisions. It is an alternative to PYTHIA and is better at modeling soft physics processes present in high energy collisions. PHOJET implements the Dual Parton model[29][30] and multiple parton interactions[31] to model soft physics. Hard interactions are implemented in PHOJET using LO scattering elements and it uses PYTHIA for the fragmentation and hadronization phase. Due to its ability to model soft physics, PHOJET is better at comparing to minimum bias[4] data and understanding jet results in a low kinematic range. PHOJET also acts as a benchmark in understanding any bias due to using other MC generators, such as PYTHIA. PHOJET v1.2 is used in this thesis.

1.5 The Quark-Gluon Plasma

1.5.1 Asymptotic Freedom and the Perfect Fluid

Hydrodynamics

The conservation laws for a relativistic fluid conserve the charge current and energy-momentum tensor of the expanding fluid such that:

$$\partial_\mu N_i^\mu = 0 \tag{1.22}$$

$$\partial_\mu T^{\mu\nu} = 0 \tag{1.23}$$

---

[4]Events with a low total transverse momentum and high cross section

1.5.2 Energy Loss in a Colored Medium

1.5.3 The Nuclear Modification Factor

1.5.4 Nuclear Collisions

1.6 QGP in Proton-Proton Collisions?

As previoulsy stated a QGP is believed to be absent in proton-proton collisions, thus any signature of a QGP should likewise be absent. However, one way of quantifying the presence of the QGP is via the Bjorken energy density.

$$\varepsilon = \frac{1}{\tau A} \frac{dE_T}{d\eta} \tag{1.24}$$

where A is the transverse area of the nuclei, τ is the proper time, and $dE_T/d\eta$ is the transverse energy per unit psuedorapidity. It can be shown that the 150 MeV critical temperature need for the phase transition to the QGP corresponds to $1 - 3 GeV/fm^3$ energy density. The quantity $dE_T/d\eta$ can be related to the mean transverse momentum $< p_T >$ and particle multiplictiy[5] per unity psuedorapidity as:

$$\frac{dE_t}{d\eta} \approx < p_T > \frac{dN}{d\eta} \tag{1.25}$$

where $< p_T >$ is the mean transverse momentum and $dN/d\eta$ is the particle multiplicity per unit psuedorapidity. This suggest that in very high multiplicity proton-proton events signatures of the QGP may be present. This is one of the most active and newest areas of research in heavy ion physics.

---

[5]Multiplicity is defined as the number of particles per event

Bibliography

[1] Michael Riordan. The discovery of quarks. *Science*, 256(5061):1287–1293, 1992. 1

[2] Frank Wilczek. Asymptotic freedom: From paradox to paradigm. *Proc. Nat. Acad. Sci.*, 102:8403–8413, 2005. [Rev. Mod. Phys.77,857(2005)]. 2

[3] Vardan Khachatryan et al. Measurement of the inclusive 3-jet production differential cross section in proton–proton collisions at 7 TeV and determination of the strong coupling constant in the TeV range. *Eur. Phys. J.*, C75(5):186, 2015. 2

[4] Jets at cms and the determination of their energy scale, July 2012. 3

[5] J. D. Bjorken. Asymptotic sum rules at infinite momentum. *Phys. Rev.*, 179:1547–1553, Mar 1969. 3

[6] J. D. Bjorken. Can We Measure Parton Parton Cross-Sections? *Phys. Rev.*, D8:4098, 1973. 3

[7] Matt Dobbs and Jorgen Beck Hansen. The HepMC C++ Monte Carlo event record for High Energy Physics. *Comput. Phys. Commun.*, 134:41–46, 2001. 5

[8] Wolfgang Kurt Hermann Panofsky. Low q electrodynamics, elastic and inelastic electron (and muon) scattering. 1968. 6

[9] J. Feltesse. Introduction to Parton Distribution Functions. *Scholarpedia*, 5(11):10160, 2010. revision #186761. 6

[10] K. Kovarik, T. Jezo, A. Kusina, F. I. Olness, I. Schienbein, T. Stavreva, and J. Y. Yu. CTEQ nuclear parton distribution functions. *PoS*, DIS2013:274, 2013. 6

[11] Richard D. Ball, Valerio Bertone, Stefano Carrazza, Christopher S. Deans, Luigi Del Debbio, Stefano Forte, Alberto Guffanti, Nathan P. Hartland, José I. Latorre, Juan Rojo, and Maria Ubiali. Parton distributions for the LHC Run II. *JHEP*, 04(arXiv:1410.8849. EDINBURGH 2014-15. IFUM-1034-FT. CERN-PH-TH-2013-253. OUTP-14-11P. CAVENDISH-HEP-14-11):040. 138 p, Oct 2014. Comments: 138 pages, 64 figures. Several typos in text and references corrected, one reference added. 6

[12] Harald Fritzsch. QCD: 20 years later. In *QCD 20 Years Later: Proceedings, Workshop, Aachen, Germany, June 9-13, 1992*, pages 827–852, 1992. 7

[13] John C. Collins, Davison E. Soper, and George F. Sterman. Factorization of Hard Processes in QCD. *Adv. Ser. Direct. High Energy Phys.*, 5:1–91, 1989. 7

[14] Nora Brambilla, Xavier Garcia i Tormo, Joan Soto, and Antonio Vairo. The Logarithmic contribution to the QCD static energy at N**4 LO. *Phys. Lett.*, B647:185–193, 2007. 7

[15] Martin Erdmann. Investigation of quark - anti-quark interaction properties using leading particle measurements in e+ e- annihilation. *Phys. Lett.*, B510:29–35, 2001. 7

[16] B. R. Webber. Hadronization. In *Proceedings: Summer School on Hadronic Aspects of Collider Physics, Zuoz, Switzerland, Aug 23-31, 1994*, pages 49–77, 1994. 8

[17] Bo Andersson, Sandipan Mohanty, and Fredrik Soderberg. Recent developments in the Lund model. In *36th Annual Winter School on Nuclear and Particle Physics (PINP 2002) and 8th St. Petersburg School on Theoretical Physics St. Petersburg, Russia, February 25-March 3, 2002*, 2002. 9

[18] B. R. Webber. A QCD Model for Jet Fragmentation Including Soft Gluon Interference. *Nucl. Phys.*, B238:492–528, 1984. 9

[19] L. L. Jenkovszky, V. K. Magas, J. T. Londergan, and A. P. Szczepaniak. Explicit Model Realizing Parton-Hadron Duality. *Int. J. Mod. Phys.*, A27:1250157, 2012. 10

[20] Jan Rak and Michael J. Tannenbaum. *QCD in hard scattering*, pages 214–243. Cambridge Monographs on Particle Physics, Nuclear Physics and Cosmology. Cambridge University Press, 2013. 10

[21] Ryan Atkin. Review of jet reconstruction algorithms. *J. Phys. Conf. Ser.*, 645(1):012008, 2015. 11, 14

[22] J E Huth, N Wainer, K Meier, N J Hadley, F Aversa, Mario Greco, P Chiappetta, J P Guillet, S Ellis, Zoltán Kunszt, and Davison Eugene Soper. Toward a standardization of jet definitions. (FERMILAB-CONF-90-249-E):7 p, Dec 1990. 11

[23] Gerald C. Blazey et al. Run II jet physics. In *QCD and weak boson physics in Run II. Proceedings, Batavia, USA, March 4-6, June 3-4, November 4-6, 1999*, pages 47–77, 2000. 11

[24] Matteo Cacciari, Gavin P. Salam, and Gregory Soyez. FastJet User Manual. *Eur. Phys. J.*, C72:1896, 2012. 15

[25] Megan Connors, Christine Nattrass, Rosi Reed, and Sevil Salur. Jet measurements in heavy ion physics. *Rev. Mod. Phys.*, 90:025005, 2018. 16

[26] R Brun, F Bruyant, M Maire, A C McPherson, and P Zanarini. *GEANT 3: user's guide Geant 3.10, Geant 3.11; rev. version*. CERN, Geneva, 1987. 16

[27] Torbjorn Sjostrand, Stephen Mrenna, and Peter Z. Skands. A Brief Introduction to PYTHIA 8.1. *Comput. Phys. Commun.*, 178:852–867, 2008. 16

[28] Peter Zeiler Skands. Tuning Monte Carlo Generators: The Perugia Tunes. *Phys. Rev.*, D82:074018, 2010. 17

[29] A. Capella, U. Sukhatme, C.-I. Tan, and J. Tran Thanh Van. Dual parton model. *Physics Reports*, 236(4):225 – 329, 1994. 17

[30] Cheuk-Yin Wong. *Introduction to high-energy heavy-ion collisions*. World Scientific, Singapore, 1994. Erratum. 17

[31] Fritz W. Bopp, R. Engel, and J. Ranft. Rapidity gaps and the PHOJET Monte Carlo. In *High energy physics. Proceedings, LAFEX International School, Session C, Workshop on Diffractive Physics, LISHEP'98, Rio de Janeiro, Brazil, February 16-20, 1998*, pages 729–741, 1998. 17

[32] C. Patrignani et al. Review of Particle Physics. *Chin. Phys.*, C40(10):100001, 2016. 25

[33] Francesco Noferini. The ALICE PID performance in Run 1 and perspectives in view of Run 2. In *Proceedings, 3rd Large Hadron Collider Physics Conference (LHCP 2015): St. Petersburg, Russia, August 31-September 5, 2015*, pages 523–528, Gatchina, 2016. Kurchatov Institute, Kurchatov Institute. 26

[34] Betty Bezverkhny Abelev et al. Production of charged pions, kaons and protons at large transverse momenta in pp and Pb–Pb collisions at $\sqrt{s_{\mathrm{NN}}}$ =2.76 TeV. *Phys. Lett.*, B736:196–207, 2014. 26

Appendices

A   Particle Identification via Bethe-Bloch

The energy loss of a relativistic charged particle traversing through a medium is given by the Bethe-Bloch relation:

$$\frac{dE}{dx} \propto \frac{1}{\beta^2} \frac{Z}{A} \rho \left[\frac{1}{2} \ln \frac{2m_e c^2 \beta^2 \gamma^2 T_{max}}{I^2} - \beta^2 - \frac{\delta(\beta\gamma)}{2} \right] \tag{26}$$

where ρ is the density of the medium, $\frac{Z}{A}$ is the ratio of the atomic number to the atomic mass of the absorber, β is the ratio of the particle's momentum to energy, T_{max} is the maximum transfer energy from the charged particle to an electron in the medium, I^2 is the mean excitation energy of the medium, $\frac{\delta(\beta\gamma)}{2}$ is a correction factor based on the polarization of the material, and γ^2 is the lorentz factor $\frac{1}{\sqrt{1-\beta^2}}$.
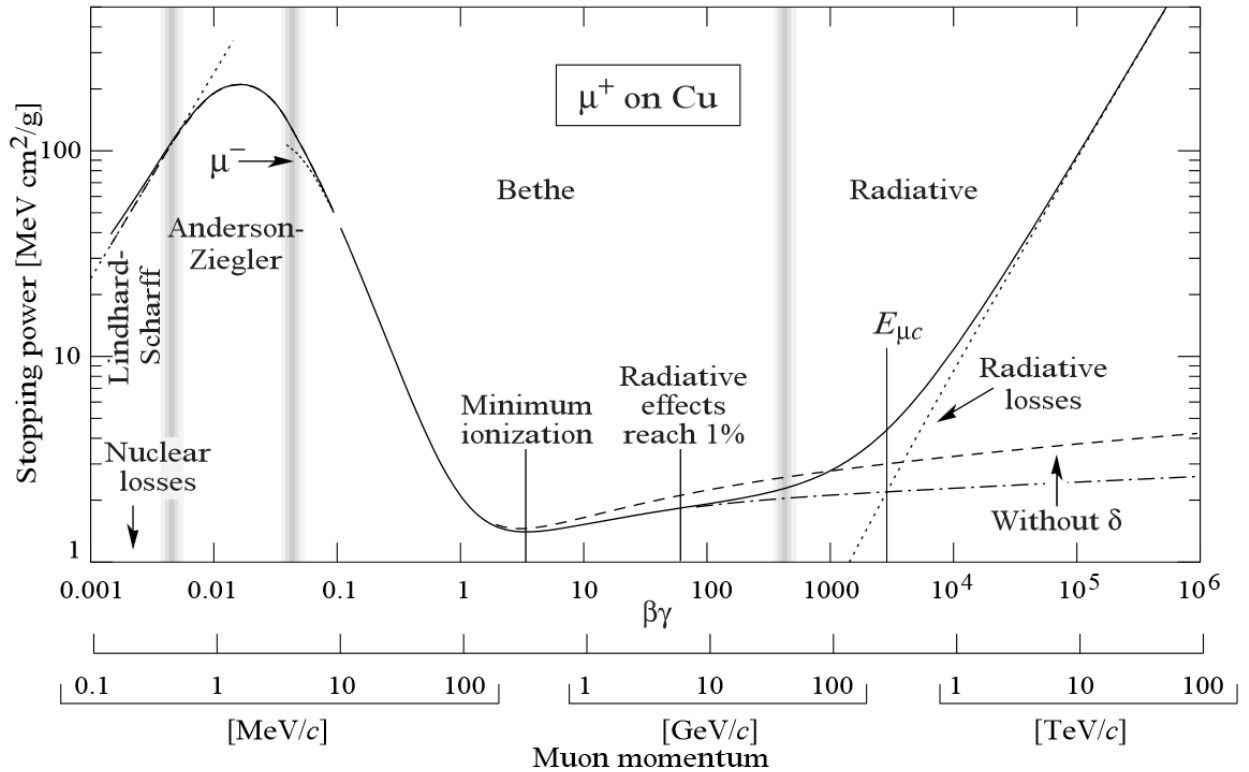

Figure 11: Energy loss of a muon traversing a copper medium between 0.1 MeV to 100 TeV [32].

Figure 11 shows the Bethe-Bloch curve for a muon over a wide kinematic range. At low energies the dominate form of energy loss is via elastic scattering, while at high energies

radiation becomes the dominate energy loss mechanism. When $\beta\gamma \approx 3$ the muon losses the least amount of energy possible and is called a minimum ionization particle(MIP).

The ALICE ITS and TPC[6] cannot directly measure the energy loss of a particle traversing either sub-detector. Instead they perform PID by measuring the relative amplitudes from the sub-detectors read-out elements, pixels in the ITS and copper pads in the TPC. The amplitudes are then fit to the Bethe-Bloch equation as seen in Figure 12. Electrons weakly obey the Bethe-Bloch relationship in the kinematic ranges sensitive to the ITS and TPC and thus have a constant energy loss in both detectors.

(a) ALICE ITS(pp $\sqrt{s} = 13$ TeV)   (b) ALICE TPC (PbPb $\sqrt{s_{NN}} = 5.02$ TeV)
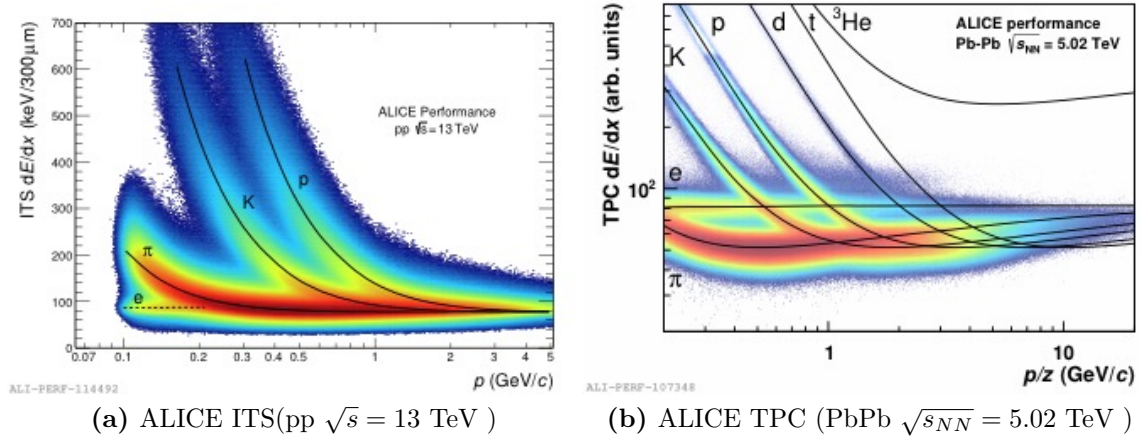
Figure 12: Specific energy loss for the ITS*(left)* and the TPC*(right)* with Bethe-Bloch fits from different particle species traversing each detector[33].

Figure 12 also shows that the Bethe-Bloch curves merge above some kinematic range, 4 GeV in the ITS and 10 GeV in the TPC. Above this kinematic range particles cannot be distinguished on a track-by-track basis, but by using statistical methods and Gaussian fits PID can be extended up to 20 GeV[34].

---

[6]See Section **??** and Section **??**

B   Summary of Stuff

some text here

B.1   More Things

some equations here

B.2   Other Aspects

some equations also here

Vita